



“Enhancing power system stability: an innovative approach using coordination of FOPID controller for PSS and SVC FACTS device with MFO algorithm”

Nader M. A. Ibrahim¹ · Ehab A. El-said¹ · Hossam E. M. Attia¹ · Bassam A. Hemade¹

Received: 16 May 2023 / Accepted: 18 September 2023
© The Author(s) 2023

Abstract

This paper investigates an optimal methodology for mitigating low-frequency oscillation concerns in power systems. The study explores the synergistic integration of a power system stabilizer (PSS) and a flexible alternating current transmission system (FACTS) to formulate an intelligent controller. A comprehensive analysis encompasses various PSS design strategies, including lead-lag (LL), proportional-derivative-integral (PID), and fractional-order proportional-integral-derivative (FOPID) controllers. The FACTS device selected for this investigation is a static VAR compensator (SVC), highlighting the exceptional efficacy of FOPID-based PSS over alternative strategies with a power oscillation damper. The study extends its scope to encompass a comparative assessment of two distinct optimization algorithms: the moth flame optimization (MFO) and the antlion optimization (ALO). The research is conducted using a single-machine infinite bus power system (SMIB) as the case study platform. A total of four diverse test scenarios are executed under varying operating conditions. The evaluation of the developed method employs six distinct performance indices to investigate the developed controller thoroughly. The outcomes reveal that the MFO-optimized FOPID-PSS and SVC controller outperforms other control schemes. This optimized configuration demonstrates substantial improvements across all performance indices. These findings underscore the superior capabilities of the proposed approach in enhancing power system stability and performance.

Keywords Coordinated control · FOPID · Low-frequency oscillation · MFO · PSS · SVC

1 Introduction

As energy demand and resource depletion increase, managing power generation becomes more complex. It now requires a fast and robust coordinated control technique. Power systems can withstand strained situations with less difficulty because of the rapid development of intelligent algorithms. The rises in electric power demand and stability requirements

in a competitive environment require more sophisticated control systems with high speed and flexibility [1–3].

Low-frequency oscillations are considered one of the most common issues regarding power system stability. LFO ranges from 0.1 to 3 Hz typically. Moreover, LFO reduces power transfer capacity and disturbs the power system operation of modern power system networks. The undesired oscillation is due to the coupling of a high gain and an inadequately tuned generator excitation system. Undamped LFOs can cause system instability problems or even a total blackout if not considered carefully. A straightforward and efficient supplementary excitation controller becomes essential to improve power system stability [4].

Researchers apply a power system stabilizer (PSS) with various structures to reduce oscillations in the electrical power system. During the increase in electrical power demand, PSS devices can improve the performance of excitation systems and maintain high-power quality standards. This improvement depends on the efficiency of the design

✉ Nader M. A. Ibrahim
nader.ibrahem@suezuni.edu.eg

Ehab A. El-said
ehab.awad@ind.suezuni.edu.eg

Hossam E. M. Attia
hossam.attia@ind.suezuni.edu.eg

Bassam A. Hemade
bassam.salama@outlook.com

¹ Electrical Power System and Machines Department, Faculty of Technology & Education, Suez University, Suez 43512, Egypt

of artificial intelligence tools in designing the PSS controller alone or in coordination with another controller [5].

Typically, PSS provides an appropriate stabilization signal under various operating conditions and disturbances [3]. In [3–6], the authors emphasize that the primary function of PSSs is to reduce generator rotor oscillations by modulating their excitation with an auxiliary stabilizing signal. A comprehensive analysis of various PSS controllers' impact on the overall dynamic performance of the power system is presented in [7]. In addition to PSS, flexible AC transmission system (FACTS) devices have received considerable attention from researchers in the last decade as essential auxiliary devices for damping power system oscillations [8].

FACTS relies mainly on rapidly developing power electronics to offer an attractive solution to many stability issues. FACTS devices can effectively improve the power transmission capacity and system stability by employing it as a power oscillation damper (POD) [9, 10]. The static VAR compensator (SVC), a widely used shunt FACTS device, can offer enough damping of the LFOs in modern networks if correctly adopted [10, 11]. The primary purpose of the SVC is to maintain bus voltages within an acceptable range. In general, if correctly coordinated with PSS, SVC can improve the damping of power system oscillations [11]. Uncoordinated controllers of both SVC and PSS can cause system instability. The coordination between SVC and PSS controllers to improve overall power system stability has received considerable attention from researchers [12, 13]. Reference [14] investigates the coordinated PSS and SVC controller for a synchronous generator.

The PSS and SVC controllers have various parameters that must be tuned. The tuning process is a large-scale, nondifferentiable, nonlinear problem. Particle swarm optimization optimized the coordinated lead-lag (LL-PSS) and PID-SVC gains [15]. Due to the rapid advancement of computer technology in recent years, it has become possible to implement power system stabilization controllers with the help of AI optimization tools. Several novel metaheuristic algorithms present the improved, coordinated design between SVC and PSS controllers [4].

Alternatively, various coordinated controller designs for both SVC and PSS to enhance the damping of LFO and improve the power system stability have been suggested in different works. In [16], PSSs and SVC damping controllers are designed using a linearized power system model for small-signal stability enhancement considering a specific operating point. In [17], a coordination controller for the single-machine infinite bus (SMIB) with SVC was designed using input–output linearization and pole assignment techniques.

Several researchers heavily rely on the traditional lead-lag controller when modeling the coordinated structure of SVC with PSS, as in [12, 13, 18–20]. In [21], a comparison has

been performed between the PID controller and LL controller for SVC to reduce power system oscillations. The results show the superiority of the SVC-based LL-power oscillation damping (LL-POD) compared to the PID-POD.

Recently, control schemes have drastically improved, which resulted in industrial advancements and special attention focused on the FOPID [1]. Unlike the PID controller, which only accepts integer values for the Laplace operator “s,” the FOPID controller accepts fraction values for the “s” operator. Therefore, the FOPID controller system is superior to other controllers. The reliability and robustness of the FOPID controllers have led to widespread implementation [22–24].

Several studies are devoted to employing various intelligent techniques to study and analyze coordinated control of SVC devices and PSS. Coordination tuning of PSS and SVC controllers using bacterial swarming optimization (BSO) is observed [25]. The study achieves proper damping of electromechanical oscillations. In [26], the author utilizes the crow search algorithm (CSA) to find the optimal coordinated SVC and PSS dynamic control of SMIB. The antlion optimizer (ALO) developed technique [27].

The PSS and FACTS-PODs controllers are tuned, considering interconnected multimachine power systems. A PSS controller parameter tuning issue in [28] utilizes a new population-based moth flame optimization (MFO) algorithm in a multimachine power system. In [28–30], there is a comparison process between the MFO, firefly algorithm (FA), and bacteria foraging (BF) in designing controllers for enhancing power system stability. The comparison results have emphasized the effectiveness of MFO in enhancing overall system stability. The MFO was suggested for optimal tuning of the PSS controller in [31] to damping LFO in electrical power systems.

The MFO applied to design the FOPID coordinated with other controllers to present novel control structures or cascade controllers to employ as automatic generation control (AGC) with different electric power system topologies [2, 32–34]. Different optimization tools are applied to design the AGC as ALO [35], MFO [36], gray wolf optimizer (GWO) [37], and grasshopper algorithm [38].

All the control structures are compared in a single-machine infinite bus system (SMIB). Four different severe short circuit tests were applied to test the designed controller. Six different performance indices analyze the test results: maximum overshoot, settling time, integral absolute of the error (IAE), integral time absolute of the error (ITAE), integral square of the error (ISE), and integral square time of the error (ISTE).

There is no single best objective function that can suit all situations. However, some standard criteria are four main types [39, 40]: eigenvalue-based objective functions [40–42], time-domain objective functions [44], frequency-domain

objective functions [45], and multi-objective functions mix the objective functions with weighting factors [46].

The time-domain objective function mainly includes ISE, ITSE, IAE, and ITAE. The ITAE as an objective function has many advantages over the other objective functions in stability studies. ITAE can improve the dynamic performance of a control system by giving more weight to the errors that occur later. ITAE can reduce the steady-state error, which is often more important than the transient response in many applications. ITAE can also result in a more robust and stable control system, especially when there are uncertainties and variations in the system parameters or operating conditions. Furthermore, ITAE can tune PID controllers more effectively than other criteria, such as ISE, because it can balance the trade-off between the proportional, integral, and derivative gains [47–49].

This work aims to increase the power system stability by utilizing the MFO to design the coordinated FOPID-PSS and SVC controller as a power oscillation damper (POD). The POD controller is an additional signal to the SVC having a FOPID control structure. The developed method will use the MFO algorithm to obtain optimal parameters for the FOPID controller. The robustness of the MFO algorithm is compared with ALO. On the other hand, the proposed method will be compared with lead-lag PID controllers to ensure the robustness of the developed technique.

The rest of the present paper is constructed as follows: power system modeling is shown in Sect. 2. Then, the controller structure is explained in Sect. Optimization techniques are presented in Sect. 4. Further, in Sect. 5, results and discussions are presented. The conclusion is shown in Sect. 6.

2 Power system modeling

2.1 Modeling of SMIB with SVC

The SMIB system consists of a synchronous generator connected to an infinite bus through a step-up transformer, followed by a transmission line divided into two equal lines connected in series. All data related to the dynamic model of SMIB are listed in [50]. The single-line diagram of the SMIB system is shown in Fig. 1. The SVC comprises a three-phase fixed capacitor thyristor-controlled reactor (FC-TCR) connected in the middle of the transmission line and in parallel with the network [21]. SVC acts as a variable reactance to control specific power system parameters, typically bus voltages. It is widely used for support for reactive power and voltage regulation [50].

In Fig. 1, the terms X_{l1} and X_{l2} refer to the transmission line reactance. Additionally, V_t and V_b refer to the voltages at the generator terminals and the infinite bus, respectively. The SVC controls bus voltage within the desired level [51].

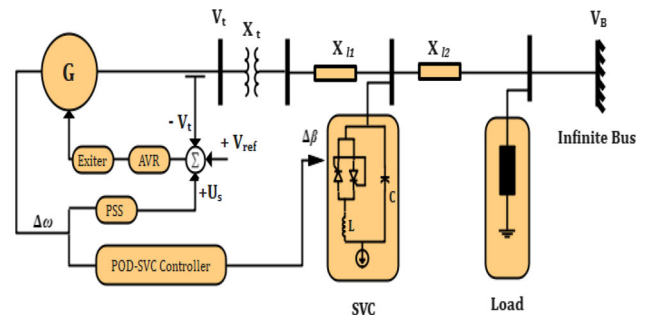


Fig. 1 Power system model of a SMIB equipped with SVC

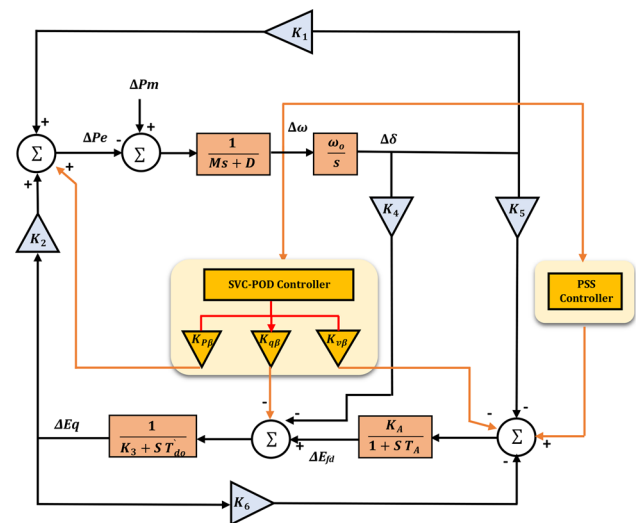


Fig. 2 Heffron–Phillips SMIB linearized model equipped with SVC

2.2 Linear Model of the SMIB with SVC Facts Device

To optimize the SVC-based power system damping controller, a fourth-order state-space model of the SMIB system with an SVC device and an IEEE Type-ST1A excitation system has been developed, as shown in Fig. 1 [52]. Generally, linearized incremental models around an equilibrium operating point are employed in the design of PSS and SVC. Therefore, the linear Heffron–Phillips model of a SMIB system with SVC can be formulated as in Eqs. (1–4) [26, 52].

Figure 2 shows the Heffron–Phillips SMIB linearized model equipped with SVC [5, 52]. In Fig. 2, K_1 – K_6 , $K_{p\beta}$, $K_{q\beta}$, $K_{v\beta}$, and T_3 are constants for the Heffron–Phillips SMIB linearized model with SVC. These constants are calculated in [3, 6, 53]. M is the inertia constant, K_A is the exciter system circuit constant, D is the coefficient of damping torque, and T_A is the exciter time constant. The whole parameters of the SMIB test system are listed in Appendix 1 [3, 6].

$$\dot{\delta} = \omega_0 \Delta\omega \tag{1}$$

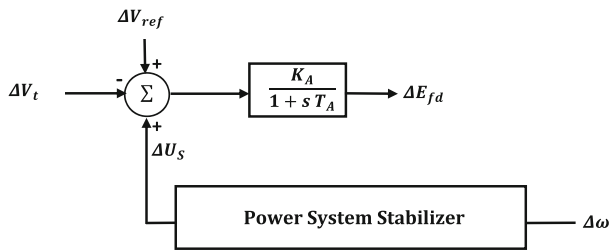


Fig. 3 IEEE type-ST1 excitation system with PSS

$$\Delta \dot{\omega} = \frac{[-K_1 \Delta \delta - K_2 \Delta \frac{E}{q} - K_P \Delta \beta_{svc} - D \Delta \omega]}{2H} \quad (2)$$

$$\Delta \frac{E}{q} = \frac{[-K_4 \Delta \delta - K_3 \Delta \frac{E}{q} - K_q \Delta \beta_{svc} + \Delta E_{fd}]}{T'_{do}} \quad (3)$$

$$\Delta \dot{E}_{fd} = \frac{[-\Delta E_{fd} - K_A (K_5 \Delta \delta + K_6 \Delta \frac{E}{q} + K_v \Delta \beta_{svc})]}{T_A} \quad (4)$$

where:

$$K_1 = \frac{\partial P_t}{\partial \delta}, K_2 = \frac{\partial P_t}{\partial \frac{E}{q}}, K_{p\beta} = \frac{\partial P_t}{\partial \beta_{svc}}$$

$$K_3 = \frac{\partial E_q}{\partial \frac{E}{q}}, K_4 = \frac{\partial E_q}{\partial \delta}, K_{q\beta} = \frac{\partial E_q}{\partial \beta_{svc}}, \quad (5)$$

$$K_5 = \frac{\partial V_t}{\partial \delta}, K_6 = \frac{\partial V_t}{\partial \frac{E}{q}}, K_{v\beta} = \frac{\partial V_t}{\partial \beta_{svc}}$$

3 Controller structure

This section discusses the three types of power system stabilizers used in the investigation. The PSS enhances the stability of the power system network by acting through the excitation system. The excitation system used in this work is based on the IEEE Type-ST1 excitation system with PSS, as shown in Fig. 3. The system is expressed by Eq. (6) [54].

$$\Delta E_{fd} = K_A (V_{ref} - V_t + U_s) - E_{fd} / T_A \quad (6)$$

where V_{ref} and V_t represent the reference and generator terminal voltages, and K_A and T_A are the excitation system amplifier gain and time constants, respectively. Typically, the stabilizer prevents the power system from oscillating after being subjected to a significant perturbation. The input signal

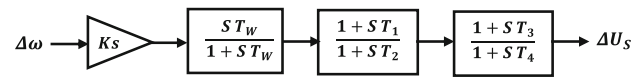


Fig. 4 The PSS-LL structure

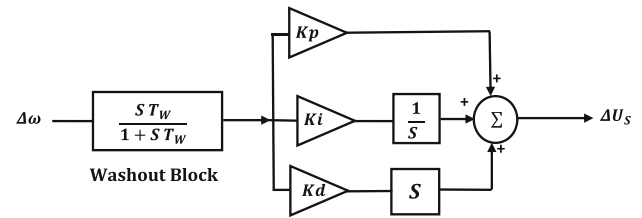


Fig. 5 The PID-PSS structure

for a PSS structure is typically a deviation from synchronous speed [55].

3.1 Lead lag-PSS.

Figure 4 shows the structure of the LL-PSS, consisting of a washout block, a gain block, and two phase-compensation blocks. The washout block acts as a high-pass filter for input gained from the gain block; it typically lasts from one to twenty seconds. The gain block controls the damping signal received from the PSS input. Two phases at different levels work together to provide the necessary phase-lead feature. The time constants for the first and second compensation phases are T_1 , T_2 , T_3 , and T_4 , respectively. The transfer function of the PSS is expressed by Eq. (7) [15].

$$G_{PSS}(s) = K_S \left[\left(\frac{ST_w}{1 + sT_w} \right) * \left(\frac{1 + sT_1}{1 + sT_2} \right) * \left(\frac{1 + sT_3}{1 + sT_4} \right) \right] \quad (7)$$

where K_s , T_1 , T_2 , T_3 , and T_4 the controller gains.

3.2 PID-PSS

Since the 1930s, three-mode controllers that work in proportional, integral, and derivative (PID) ways have been used for various industrial applications. The PID controller transfer function is represented by Eq. (8). K_p , K_i , and K_d are the controller gains. The structure of the PID-PSS considered in this work is shown in Fig. 5. [56].

$$G_{PSS}(s) = K_p + \frac{K_i}{s} + K_d s \quad (8)$$

3.3 FOPID-PSS

Podlubny has proposed a modification to the PID control system, commonly known as a fractional-order PID controller,

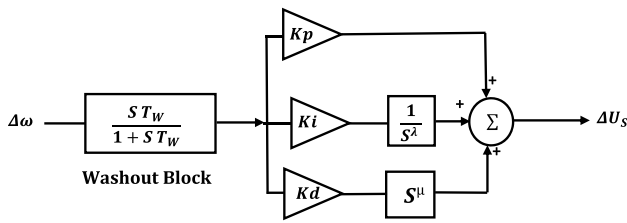


Fig. 6 The FOPID-PSS structure

due to the inclusion of the differentiator of order (μ) and integrator of order (λ). Therefore, the FOPID controller has a higher stability range than the PID controller. This $PI^{-\lambda}D^{\mu}$ is a highly multilateral control system that allows fine-tuning. The modification led to a more robust control system with distinguishable dynamic characteristics [22]. The differential equation and the transfer function for the $PI^{-\lambda}D^{\mu}$ controller are given by Eq. (9) and (10) [1, 22].

$$U(t) = K_p e(t) + K_i D^{-\lambda} e(t) + K_d D^{\mu} e(t) \tag{9}$$

$$G_{PSS}(s) = K_p + K_i S^{-\lambda} + K_d S^{\mu}, \lambda, \mu > 0 \tag{10}$$

The block diagram of the FOPID controller is shown in Fig. 6, where $K_i, K_d, K_p, \lambda,$ and μ represent the proportional, differential, integral constants, fractional-order integral, and fractional-order derivative elements, respectively [1].

3.4 SVC-POD controller

In order to maintain or regulate specific power system variables, the SVC device is commonly used. SVC is a shunt-connected VAR generator or load. Typically, the bus voltage is the controlled variable; however, oscillation damping can also be achieved by superimposing an additional stabilizing signal and supplementary control on the SVC voltage control loop. The configuration of an SVC, particularly that of an FC-TCR, is illustrated in the schematic diagram of Fig. 7 [14]. The power oscillation damper (POD) controller was added to the SVC to increase the system stability with the PSS. The POD structure is also like the proposed PSS FOPID. A proportional-integral (PI) controller regulates this firing angle, maintaining the bus voltage at the reference (V_{ref}) value [6, 21, 57, 58]. As a function of the SVC switch firing angle ($90^{\circ} \leq \alpha \leq 180^{\circ}$), the inductive susceptance of the thyristor-controlled reactor (β_{TCR}) can be determined using Eq. (11) and (12). Consequently, Eq. (13) can be used to determine the SVC effective reactance (X_{SVC}). Hence, the SVC equivalent susceptance (β_{SVC}) can be calculated using Eq. (14) [46–48].

$$\beta_{TCR} = \frac{1}{X_L} \frac{(2\pi - 2 - \sin(2))}{\pi} \tag{11}$$

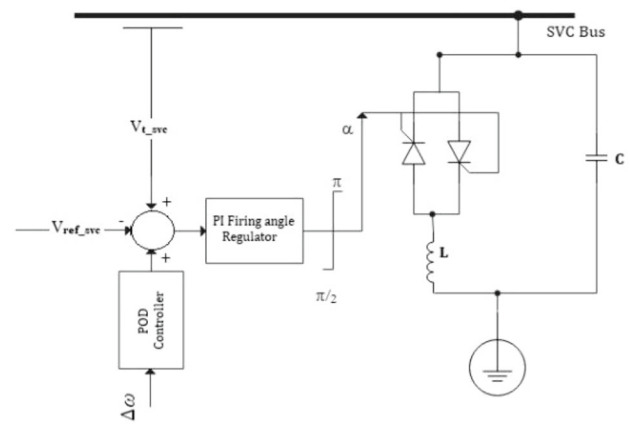


Fig. 7 The schematic diagram of SVC-FCTCR [6, 21, 57, 58]

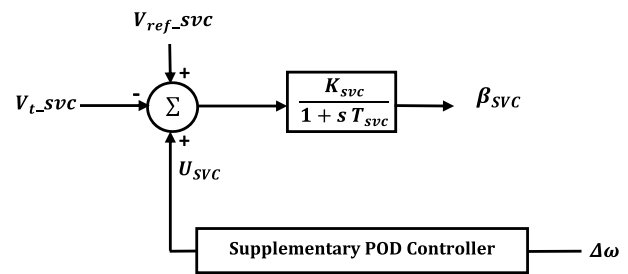


Fig. 8 Block diagram of the POD-SVC controller

$$X_{TCR} = \frac{1}{\beta_{TCR}} = X_L \frac{\pi}{[2(-\pi) - \sin(2)]} \tag{12}$$

$$X_{SVC} = \frac{X_C X_{TCR}}{X_{TCR} - X_C} = \frac{\pi X_L X_C}{X_C [2(-\pi) - \sin(2)] + \pi X_L} \tag{13}$$

$$\beta_{SVC} = \frac{1}{X_{SVC}} = \frac{X_C [2(-\pi) - \sin(2)] + \pi X_L}{\pi X_L X_C} \tag{14}$$

where X_C denotes thyristor-switched capacitor (TSC) reactance, and X_L represents thyristor-controlled reactor (TCR) reactance. The output signal (susceptance provided by SVC (β_{svc})) as a function of change in speed is considered in this work. The SVC and its firing control system can be described by Eq. (15) [26].

$$\dot{\beta}_{SVC} = \frac{[K_{svc}(-V_{t_svc} + V_{ref_svc} + U_{svc}) - \beta_{svc}]}{T_{svc}} \tag{15}$$

where β_{svc} is the SVC equivalent susceptance, V_{t_svc} is the bus voltage magnitude, V_{ref_svc} is the reference voltage for the SVC, and U_{svc} is the supplemental control input. The gain and time constant of the SVC regulator is K_{svc} and T_{svc} , respectively. Figure 8 shows the block diagram for the SVC with the supplementary damping controller [62]. This work

will use the FOPID controller with the SVC device as a POD unit to enhance power oscillation damping.

3.5 Objective function

Considering power system oscillations, the PSS and SVC controller gains can be adjusted to minimize the overshoot and settling time. Consequently, the power system oscillation will be damped, increasing power system dynamic stability. This research aims to simultaneously tune the gains of the PSS and SVC controllers to achieve optimum system stability. Therefore, the performance index ITAE (integral time absolute error) was employed as an objective function, as shown in Eq. (16).

$$J = \int_{t=0}^{t=t_{sim}} |\Delta\omega| dt \tag{16}$$

where t_{sim} is the simulation time, and $\Delta\omega$ is the speed deviation. The system response can be improved by minimizing this objective function [13, 63].

3.6 Stability performance index

Four performance indices are considered in different scenarios to evaluate controller performance. These indices are the integral of square error (ISE), the integral of absolute error (IAE), the integral of time absolute error (ITAE), and the integral of square absolute error (ISAE). The four indices are mathematically formulated as in [24].

The optimal set of PSS and SVC-based damping controller gains in this study are obtained using ALO and MFO algorithms. The following section is a brief overview of the ALO and MFO techniques. Table 1 shows the typical ranges of the

Table 1 Controllers optimized gains typical ranges

Controller	Controller gains					
LL- PSS	Ks	T1	T2	T3	T4	
	Min	0.01	0.01	0.01	0.01	0.01
	Max	10	1	1	1	1
PID-PSS	Kp	Ki	Kd	–	–	
	Min	0.01	0.01	0.01	–	–
	Max	10	10	10	–	–
FOPID-PSS	Kp	Ki	Kd	λ	μ	
	Min	0.01	0.01	0.01	0.01	0.01
	Max	10	10	10	1	1
FOPID-SVC	Kp	Ki	Kd	λ	μ	
	Min	0.01	0.01	0.01	0.01	0.01
	Max	50	30	20	1	1

Bold values indicate the proposed data

optimized parameters. The time constant T_w is considered 20.0 s in this study.

4 Optimization techniques

4.1 Antlion optimizer

The ALO algorithm is inspired by how antlions naturally forage during ant hunting. The ant’s random walk positions are offered in Eq. (17) [29].

$$M_{Ant} = \begin{bmatrix} A_{1,1} & \cdots & A_{1,d} \\ \vdots & \ddots & \vdots \\ A_{n,1} & \cdots & A_{n,d} \end{bmatrix} \tag{17}$$

where (n) refers to the number of ants, and (d) refers to the number of variables. The locations of all antlions in the traps across search space were recorded in Eq. (18) [29, 64].

$$M_{Antlion} = \begin{bmatrix} AL_{1,1} & \cdots & AL_{1,d} \\ \vdots & \ddots & \vdots \\ AL_{n,1} & \cdots & AL_{n,d} \end{bmatrix} \tag{18}$$

In their exploration of the search space, the ants use Eq. (19) for random walks [30, 43].

$$X_i^t = \frac{(X_i^t - a_i) * (d_i - c_i^t)}{(d_i^t - a_i)} + c_i \tag{19}$$

The mathematical equation determining how ants trap antlions is given in Eqs. 20 and 21) [29, 64, 65].

$$c_i^t = Antlion_j^t + c^t \tag{20}$$

$$d_i^t = Antlion_j^t + d^t \tag{21}$$

where $Antlion_j^t$ is the position of the chosen j th antlion at t th iteration, c^t is the minimum value for all variables at t th iteration, d^t is the maximum value for all variables at t th iteration, C_i^t is the minimum of i th variable at t th iteration, and d_i^t is the maximum of i th variable at t th Iteration. The antlions will attempt to slide the ants against them once they are inside the trap by shooting the sand outward from the trap’s center.

The ant will finally fit more than the antlion. This process occurs when the antlion catches the ant in the trap deeply. Later, the antlion will adjust its position to suit the position of the hunted ant. Thus, the chances of the following hunt will be improved, the position update can be expressed as in

Algorithm (1): Pseudo-code of the ALO Algorithm.

```

Initialize the ALO Parameter (No. of search agents, Population size)
Assign the positions of ants and antlions randomly within the search space.
Find the objective function value for the ants and antlions.
Find the best antlions and assume it as elite.
While the end criterion is not satisfied
  for every ant
    Select the Position of the antlion using a roulette wheel.
    create and normalize random walk.
    Update the position of ant and antlion.
  end for
  Calculate the objective function value of all ants.
  Replace an antlion with its corresponding ant if it becomes best fitter
  value.
  Update elite with the best fitter value of an antlion
end while
Return elite

```

Fig. 9 The ALO algorithm pseudo-code

Eq. (22) for the next iteration [29, 51].

$$Ant_j^t = (R_A^t + R_E^t) / 2 \tag{22}$$

where R_E^t is the random walk around the elite at the t th iteration, and R_A^t is the random walk around the chosen antlion at the t th iteration. Figure 9 provides the pseudo-code representation of the ALO algorithm [66].

4.2 Moth flame optimization algorithm

The MFO algorithm is another nature-inspired algorithm used to determine the coefficients of suggested controllers. The MFO algorithm is based on the flying characteristics of a moth [67]. Typically, the algorithm consists of three components: the moth (M), their fitness values (OM), and flames (F), which represent the recent best position of each fitness value, whereas flames are the best solutions. Moths are the search agents that explore the solution space. As a result, the flame is considered a flag that the best moths have raised. All moths search around the flame and shift the flame to a new position if a better solution is found [31, 67].

The general organization of the MFO procedure, which incorporates the three-tuple approximation function, can be expressed as in Eq. (23). A random population of moths is generated using the initialization function I, and the values of the corresponding objective function are illustrated in Eqs. (24) and (25), respectively [29, 67].

$$MFO = (I, P, T) \tag{23}$$

$$M(i, j) = (ub(i) - lb(i)) * rand() + lb(i) \tag{24}$$

$$OM = FitnessFunction(M) \tag{25}$$

Table 2 Hyper parameters of ALO and MFO algorithms

Parameter	Setting
Search agents size	50
Maximum iterations	20
Lower (lb) and upper (ub) boundary	As in Table 1
Dimensions (d) (number of controller variables)	4: for Lead-Lag Controller. 3: for PID Controller. 5: for FOPID Controller. 10: for Coordinated FOPID-PSS&SVC

where $ub(i)$ and $lb(i)$ define the upper and lower bounds, respectively, P is a procedure that searches for neighbor solutions of the moths until the termination condition T is met. T is the procedure that returns whether or not the termination condition has been met. Based on Eq. (26), the moth updates its position regarding the flame [30, 67, 68].

$$M_i = S(M_i, F_j) \tag{26}$$

M_i denotes the position of the i th moth, and F_j denotes the j th position of the flame. Consequently, the moth's logarithmic spiral is composed as in Eq. (27) [30, 67, 68].

$$S(M_i, F_j) = D_i * e^{bt} * \cos(2Bt) + F_j \tag{27}$$

where (t) is a random number $[-1, 1]$, b is the constant shape of the logarithmic spiral, and D_i is the distance between the i th moth and the j th flame, which is to be minimized and can be determined by Eq. (28).

$$D_i = |F_j - M_i| \tag{28}$$

The mathematical definition of the adaptive mechanism to solve the number of flames during each iteration can be expressed as in Eq. (29) [31, 46, 47].

$$flame_no = round\left(N - l * \frac{N - 1}{T}\right) \tag{29}$$

where N is the maximum number of flames, l is the current iteration, and T is the maximum number of iterations (Table 2). The algorithm pseudo-code representation is shown in Fig. 10 [30, 31, 67–69].

The values of the initial parameters of the ALO and MFO algorithms are listed in Table 3.

Algorithm (2): Pseudo-code of the MFO Algorithm.

```

Input: Max_iter, n (No. of Moths), d (No. of Dimensions).
Initialize the position moths.
While l ≤ Max_iter
    Update Flame No using Eq.29
    OM = FitnessFunction(M)
    if l == 1 then
        F = sort (M); OF = sort (OM);
    else
        F = sort (Ml-1, Ml); OF = sort (OMl-1, OMl);
    end if
    for i = 1: n
        for j = 1: d
            Update r and t, where: t is a random number between -1 and 1.
                                r is the linearly decreased from -1 to -2.
            Calculate Di using Eq.28 with respect to the corresponding moths.
            Update S(Mi, Fj) using Eq.27 with respect to the corresponding m m
        end for
    end for
end while
Output: Approximated global solution.
    
```

Fig. 10 The MFO algorithm pseudo-code

Table 3 The three operating conditions active and reactive power values

Case No.	Active power (Pe) in p.u	Reactive power (Qe) in p.u
1	0.95	0.065
2	0.7	-0.29
3	0.5	-0.34

5 Results and discussions

5.1 System setup

Experimental evaluation of the proposed coordinated controller has been performed using the MATLAB Simulink model. The Simulink model and static VAR compensator (SVC) parameters are shown in Fig. 11, as listed in [59].

The MATLAB Simulink model has been modified to fit this study. These modifications can be summarized as follows:

- Machine No.2 is set as an infinite bus with a large capacity.
- Replacing the default PSS controller with the modified controller.
- Changing the SVC mode from the “VAR control (fixed susceptance)” mode of operation to the “voltage regulation,” and
- Adding the proposed power oscillation damping controller (FOPID-POD) to vary the SVC equivalent susceptance in response to the deviation of synchronous speed.

The transmission line length is 700 km, and the generator capacity is 1 GVA, where the generator is assumed to be hydro salient with 32 pairs of poles.

5.2 Simulation results

In this section, the results of the numerical investigation will be discussed. The SMIB system and the attached SVC device, as shown in Fig. 11, are simulated using MATLAB

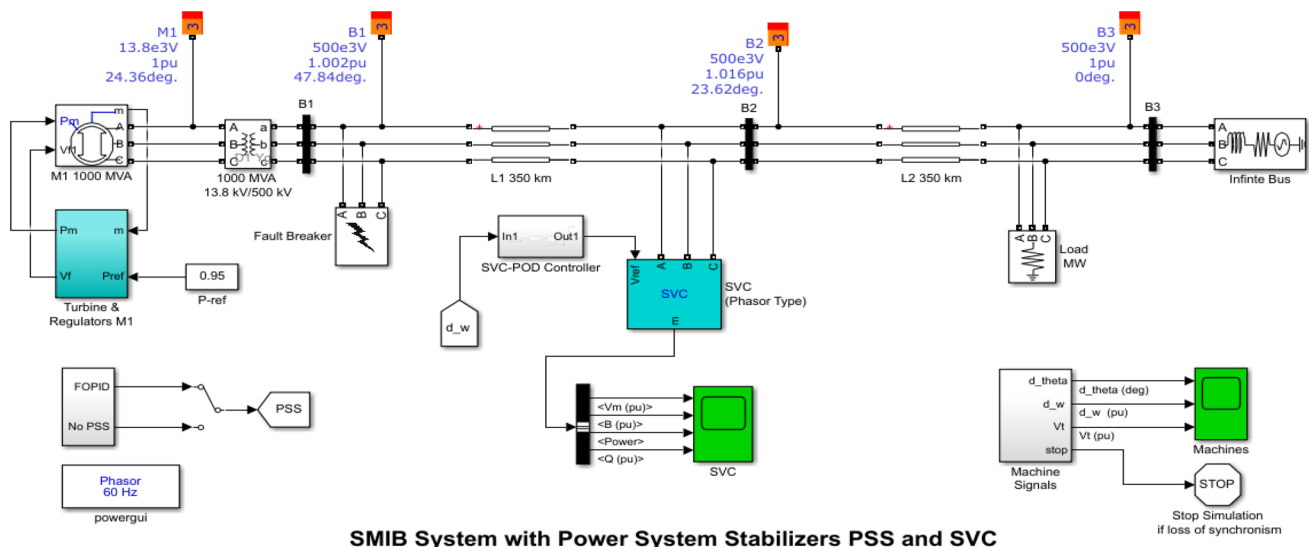


Fig. 11 Dynamic test Simulink model

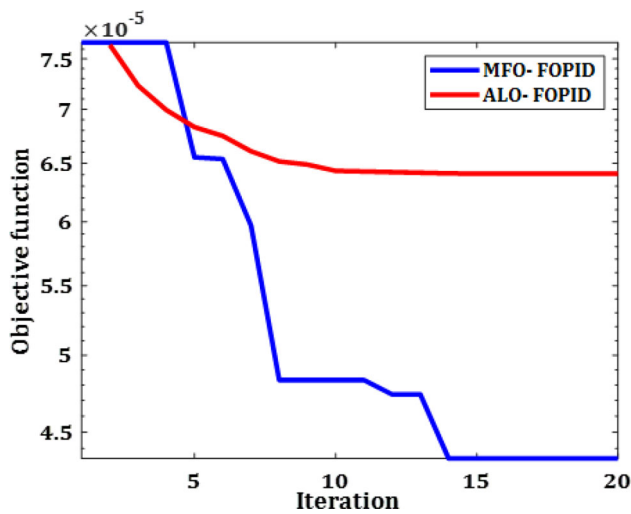


Fig. 12 Comparative convergence curves for proposed stabilizers FOPID-PSS at case No. 3

Simulink. Conventional LL-PSS, PID-PSS, and FOPID-PSS are considered for comparative purposes to verify the proposed method’s effectiveness. In this study, the performance of the SMIB system with a FOPID-PSS controller is compared to PID-PSS and LL-PSS control.

In addition, the performance of SMIB with and without SVC is also investigated. Three cases with various operating conditions are simulated, as shown in Table 3. Based on the nominal operating condition and other system parameters shown in Appendix A, MATLAB M-file has been used to obtain the complete Heffron–Phillips model parameter. These parameters will be used in the optimization process later.

The gains of the FOPID-PSS, PID-PSS, LL-PSS, and the proposed FOPID controllers for PSS and SVC are optimized using the MFO algorithm. The results obtained using the

Table 5 Testing scenarios map

Test types	Operating conditions		
	Case No.1	Case No.2	Case No.3
L-G faults occurring at the 100-km T.L	Scenario No. 1	Scenario No. 5	Scenario No. 9
L-G faults at the generator terminal	Scenario No. 2	Scenario No. 6	Scenario No. 10
LL-G faults at the generator terminal	Scenario No. 3	Scenario No. 7	Scenario No. 11
LLL-G faults at the generator terminal	Scenario No. 4	Scenario No. 8	Scenario No. 12

MFO algorithm were compared to ALO algorithms. The convergence rate of the objective function for the MFO-PSS and ALO-PSS with FOPID control designs is summarized in Fig. 12. It is worth mentioning that Case No.3 shows that the final value of the objective function (J) resulting from MFO-PSS was found to be much better than that achieved by using ALO-PSS. The final solution of the optimized parameters and optimal objective function values for the proposed stabilizers under case No.1 is reported in Table 4.

As shown in Table 5, all of the suggested stabilizers were tested against different types of disturbances. Different loading conditions have also been taken into consideration. Thus, twelve different scenarios are addressed and simulated concerning faults on the power transmission line.

Table 4 Optimization result at Case 1

Controller	PSS Gain										Cost
	K_s	T_1	T_2	T_3	T_4	$K_p(p)$	$K_i(p)$	$K_d(p)$	$\lambda(p)$	$\mu(p)$	
ALO-LL	10	0.2	0.12	0.2	0.13	–	–	–	–	–	7.63E-05
MFO-LL	10	0.2	0.06	0.01	0.06	–	–	–	–	–	7.43E-05
ALO-PID	–	–	–	–	–	10	2.39	3.71	–	–	9.43E-05
MFO-PID	–	–	–	–	–	10	0.25	3.02	–	–	9.38E-05
ALO-FOPID	–	–	–	–	–	10	5.72	9.73	0.68	0.22	1.66E-05
MFO-FOPID	–	–	–	–	–	9.99	7.69	9.73	0.28	0.32	1.22E-05

Controller	PSS Gain					SVC Gain					Cost
	$K_p(p)$	$K_i(p)$	$K_d(p)$	$\lambda(p)$	$\mu(p)$	$K_p(s)$	$K_i(s)$	$K_d(s)$	$\lambda(S)$	$\mu(s)$	
MFO-FOPID-PSS-SVC	9.63	9.99	10	0.01	0.11	44.02	30	8.03	0.28	0.39	6.81E-06

Bold values indicate the proposed data

Table 6 Performance index values at Case 1

Test scenario no	Controller	Performance indices					
		Settling time (s)	Overshoot (pu)	IAE	ITAE	ISE	ITSE
1	ALO-Lead Lag	9.9981	0.2408	3.20E-03	0.0201	4.72E-06	2.76E-05
	MFO-Lead Lag	9.2645	0.2519	3.00E-03	0.0185	4.48E-06	2.61E-05
	ALO-PID	11.3536	0.2327	3.50E-03	0.0235	4.55E-06	2.72E-05
	MFO-PID	10.4925	0.2259	3.10E-03	0.0198	3.77E-06	2.22E-05
	ALO-FOPID	7.5605	0.2243	2.10E-03	0.0122	3.42E-06	1.93E-05
	MFO-FOPID	7.6016	0.2025	1.80E-03	0.0101	2.49E-06	1.39E-05
	MFO-FOPID-PSS-SVC	6.2093	0.1475	5.12E-04	0.0026	3.39E-07	1.78E-06
2	ALO-Lead Lag	9.5926	0.4448	4.70E-03	0.0295	1.03E-05	5.97E-05
	MFO-Lead Lag	9.3474	0.4088	4.60E-03	0.0283	1.02E-05	5.93E-05
	ALO-PID	10.7245	0.4801	4.80E-03	0.0315	9.65E-06	5.62E-05
	MFO-PID	9.9912	0.48	4.80E-03	0.0309	9.83E-06	5.71E-05
	ALO-FOPID	7.6701	0.4092	3.60E-03	0.0212	9.56E-06	5.41E-05
	MFO-FOPID	7.7418	0.4092	3.50E-03	0.0204	9.18E-06	5.17E-05
	MFO-FOPID-PSS-SVC	6.3800	0.3530	1.40E-03	7.30E-03	2.13E-06	1.13E-05
3	ALO-Lead Lag	10.5171	0.9683	1.29E-02	0.0844	6.38E-05	3.90E-04
	MFO-Lead Lag	9.6681	0.8795	1.11E-02	0.071	5.20E-05	3.12E-04
	ALO-PID	11.4458	0.9685	1.46E-02	0.1008	6.92E-05	4.36E-04
	MFO-PID	11.1792	0.9685	1.42E-02	0.0967	6.8722E-05	4.30E-04
	ALO-FOPID	7.8893	0.8797	8.90E-03	0.0527	5.10E-05	2.95E-04
	MFO-FOPID	7.3368	0.8793	8.00E-03	0.0469	4.53E-05	2.60E-04
	MFO-FOPID-PSS-SVC	7.0999	0.8596	5.40E-03	0.0305	2.44E-05	1.35E-04
4	ALO-Lead Lag	10.0344	0.9651	1.25E-02	0.0819	6.17E-05	3.75E-04
	MFO-Lead Lag	9.71	0.9167	1.17E-02	0.0752	5.69E-05	3.42E-04
	ALO-PID	11.3969	0.9651	1.42E-02	0.0975	6.67E-05	4.18E-04
	MFO-PID	10.9928	0.9168	1.17E-02	0.0779	5.02E-05	3.05E-04
	ALO-FOPID	7.9103	0.9167	9.30E-03	0.0555	5.58E-05	3.24E-04
	MFO-FOPID	7.3218	0.9167	8.40E-03	0.049	4.91E-05	2.82E-04
	MFO-FOPID-PSS-SVC	7.107	0.9154	5.80E-03	0.0325	2.768E-05	1.53E-04

Bold values indicate the proposed data

Table 7 Performance index values at Case 2

Test scenario no.	Performance indices						
	Controller	Settling time (s)	Overshoot (pu)	IAE	ITAE	ISE	ITSE
5	ALO-Lead Lag	9.6931	0.2945	3.40E-03	0.0213	5.24E-06	3.13E-05
	MFO-Lead Lag	9.1774	0.2582	2.90E-03	0.0178	4.07E-06	2.39E-05
	ALO-PID	10.9478	0.2025	3.30E-03	0.0223	4.08E-06	2.45E-05
	MFO-PID	10.2196	0.2243	3.00E-03	0.0195	3.91E-06	2.32E-05
	ALO-FOPID	6.9752	0.2093	1.70E-03	0.0096	2.56E-06	1.43E-05
	MFO-FOPID	7.5888	0.1756	1.60E-03	0.009	2.00E-06	1.12E-05
	MFO-FOPID-PSS-SVC	7.1149	0.1211	1.00E-03	0.0054	8.82E-07	4.79E-06
6	ALO-Lead Lag	9.7433	0.3357	4.10E-03	0.0261	7.73E-06	4.59E-05
	MFO-Lead Lag	9.2346	0.3117	3.90E-03	0.0247	6.97E-06	4.07E-05

Table 7 (continued)

Test scenario no.	Performance indices						
	Controller	Settling time (s)	Overshoot (pu)	IAE	ITAE	ISE	ITSE
7	ALO-PID	10.9889	0.2776	4.00E-03	0.0259	6.40E-06	3.77E-05
	MFO-PID	10.2547	0.277	3.80E-03	0.0233	5.92E-06	3.51E-05
	ALO-FOPID	7.093	0.2823	2.60E-03	0.0146	5.66E-06	3.17E-05
	MFO-FOPID	6.9153	0.2772	2.40E-03	0.0139	5.32E-06	2.97E-05
	MFO-FOPID-PSS-SVC	6.8565	0.2155	1.70E-03	0.0089	2.22E-06	1.22E-05
	ALO-Lead Lag	10.3251	0.687	1.01E-02	0.0651	3.95E-05	2.39E-04
	MFO-Lead Lag	9.3171	0.6871	7.80E-03	0.0481	2.99E-05	1.73E-04
	ALO-PID	9.1585	0.7508	6.80E-03	0.0428	2.37E-05	1.35E-04
	MFO-PID	9.7283	0.6606	6.30E-03	0.0384	2.21E-05	1.27E-04
	ALO-FOPID	7.9548	0.6246	6.10E-03	0.0364	2.37E-05	1.33E-04
8	MFO-FOPID	8.0221	0.6243	5.90E-03	0.0347	2.18E-05	1.23E-04
	MFO-FOPID-PSS-SVC	6.8934	0.5982	3.90E-03	0.0217	1.25E-05	6.92E-05
	ALO-Lead Lag	9.8979	0.6583	9.00E-03	0.0579	3.27E-05	1.96E-04
	MFO-Lead Lag	9.2874	0.6583	7.00E-03	0.0433	2.48E-05	1.43E-04
	ALO-PID	9.1751	0.8263	6.60E-03	0.0413	2.60E-05	1.46E-04
	MFO-PID	9.729	0.6582	6.50E-03	0.0396	2.01E-05	1.16E-04
	ALO-FOPID	7.9848	0.6583	6.30E-03	0.0372	2.49E-05	1.42E-04
	MFO-FOPID	8.0193	0.6581	6.00E-03	0.0353	2.28E-05	1.29E-04
	MFO-FOPID-PSS-SVC	6.8861	0.6551	4.10E-03	0.0226	1.38E-05	7.61E-05

Bold values indicate the proposed data

Table 8 Performance index values at Case 3

Test scenario no	Performance indices (PI)						
	Controller	Settling time (s)	Overshoot (pu)	IAE	ITAE	ISE	ITSE
9	ALO-Lead Lag	10.1796	0.2189	2.70E-03	0.0177	3.20E-06	1.93E-05
	MFO-Lead Lag	9.7727	0.2054	2.40E-03	0.0155	2.64E-06	1.57E-05
	ALO-PID	10.2032	0.1987	2.40E-03	0.0154	2.61E-06	1.54E-05
	MFO-PID	10.4469	0.1611	2.00E-03	0.0125	1.83E-06	1.06E-05
	ALO-FOPID	8.8149	0.1683	1.70E-03	0.0106	1.73E-06	9.99E-06
	MFO-FOPID	8.7499	0.144	1.50E-03	0.0092	1.30E-06	7.50E-06
	MFO-FOPID-PSS-SVC	7.2781	0.1225	1.00E-03	0.0054	7.91E-07	4.33E-06
10	ALO-Lead Lag	10.2149	0.2518	3.30E-03	0.0211	4.52E-06	2.71E-05
	MFO-Lead Lag	9.8246	0.2419	3.10E-03	0.0194	4.13E-06	2.45E-05
	ALO-PID	10.175	0.207	2.60E-03	0.0167	3.31E-06	1.92E-05
	MFO-PID	9.7723	0.1851	2.30E-03	0.0145	2.85E-06	1.63E-05
	ALO-FOPID	8.8016	0.1992	2.20E-03	0.0133	2.90E-06	1.66E-05
	MFO-FOPID	8.7824	0.1827	2.10E-03	0.0128	2.59E-06	1.48E-05
	MFO-FOPID-PSS-SVC	7.3516	0.1546	0.0014	0.0078	1.515E-06	8.39E-06
11	ALO-Lead Lag	10.2849	0.4283	5.80E-03	0.0375	1.36E-05	8.14E-05
	MFO-Lead Lag	9.827	0.4281	4.90E-03	0.0309	1.15E-05	6.66E-05

Table 8 (continued)

Test scenario no	Controller	Performance indices (PI)					
		Settling time (s)	Overshoot (pu)	IAE	ITAE	ISE	ITSE
12	ALO-PID	9.484	0.429	4.20E-03	0.0261	9.39E-06	5.35E-05
	MFO-PID	10.2495	0.4288	4.10E-03	0.0259	8.64E-06	4.90E-05
	ALO-FOPID	8.678	0.4249	3.80E-03	0.0227	8.80E-06	4.98E-05
	MFO-FOPID	8.6216	0.4247	3.50E-03	0.021	7.92E-06	4.46E-05
	MFO-FOPID-PSS-SVC	7.3711	0.4026	2.70E-03	0.015	5.83E-06	3.22E-05
	ALO-Lead Lag	10.2687	0.4494	5.90E-03	0.0378	1.40E-05	8.33E-05
	MFO-Lead Lag	9.8057	0.4494	4.90E-03	0.0306	1.14E-05	6.59E-05
	ALO-PID	9.4567	0.4494	4.10E-03	0.0251	9.13E-06	5.17E-05
	MFO-PID	9.5854	0.4493	3.90E-03	0.0238	8.34E-06	4.69E-05
	ALO-FOPID	8.6528	0.4494	3.80E-03	0.0226	8.93E-06	5.03E-05
	MFO-FOPID	8.5668	0.4493	3.60E-03	0.0212	8.18E-06	4.59E-05
	MFO-FOPID-PSS-SVC	7.3424	0.4465	2.80E-03	0.0154	6.255E-06	3.44E-05

Bold values indicate the proposed data

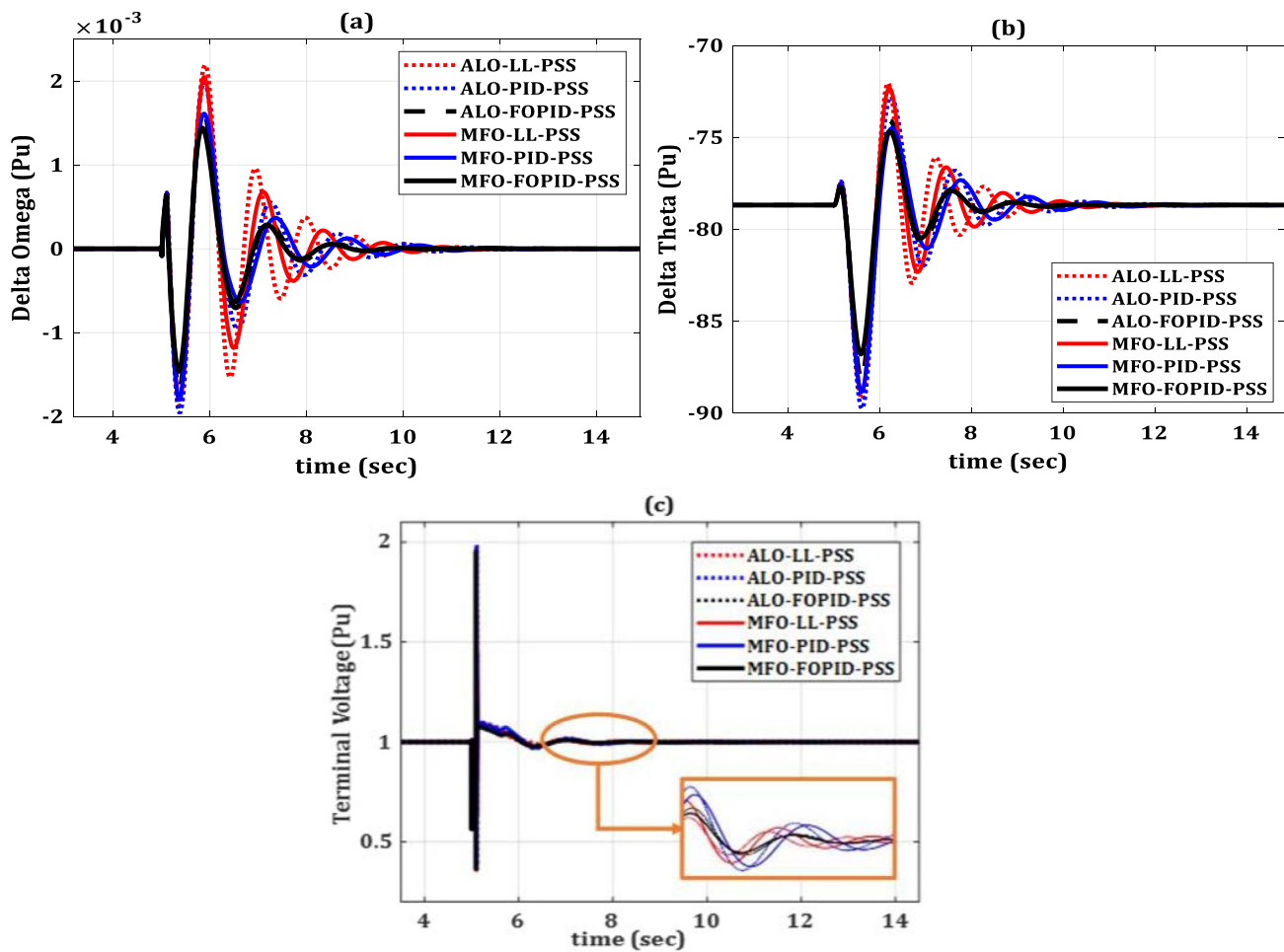


Fig. 13 Response of $\Delta\omega$, $\Delta\delta$, and $V_t(p.u.)$ to test scenario No. 9

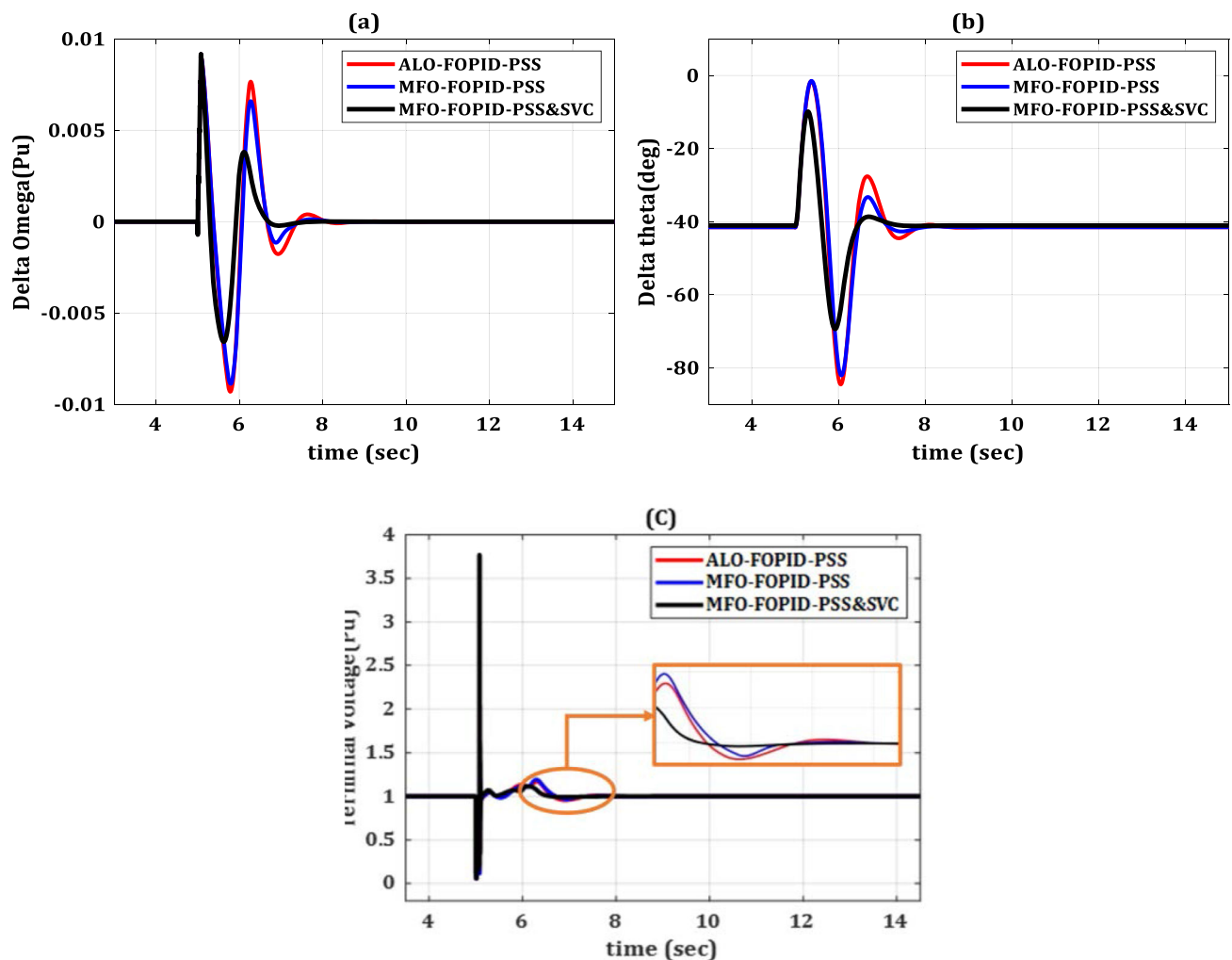


Fig. 14 Response of $\Delta\omega$, $\Delta\delta$, and V_t (p.u.) to test scenario No. 4

The scenarios considered involve a single-line-to-ground (L-G) fault set to occur 100 km from the generation unit. Moreover, different faults have also been covered, including double-line-to-ground (LL-G) and three-line-to-ground (LLL-G) faults at the generation unit terminal. All scenarios were applied individually at $t = 5$ s from the simulation starting, lasting for 100 ms.

The robustness of the proposed coordinated controller was evaluated through a performance analysis, which is achieved by using a group of performance indices. These indices are settling time, overshoot, IAE, ISE, ITAE, and ITSE. Tables 6, 7, and 8 summarize the values of the adopted performance indices for each test scenario of the proposed coordinated design MFO-FOPID-PSS&SVC compared with FOPID-PSS, PID-PSS, and LL-PSS. MFO and ALO algorithms have been used to tune the gains of all controllers to ensure a fair comparison.

The effectiveness of the performance of the proposed FOPID-PSS controller without SVC-POD under insignificant disturbance is verified by applying an L-G fault at

100 km of transmission line away from the generator unit (test scenario No. 9). Figure 13 shows the signal of both $\Delta\omega$ and $\Delta\delta$ of the generator in the responses of multiple controllers under investigation (FOPID-PSS, PID-PSS, and LL-PSS). The gains of these controllers were adjusted using MFO and ALO algorithms. As can be seen from the figure, the FOPID-PSS controller has effectively reduced the settling time and damping power system oscillations. Furthermore, the results reported in Fig. 13 show that the MFO algorithm has fewer oscillations than other optimization-based controllers. MFO is much quicker than the ALO algorithm for all PSS control structures. Consequently, it can be concluded that the proposed MFO-FOPID-PSS controller has a superior response over the other stabilizers.

Moreover, some of the test scenarios in different case studies will be discussed in detail in the following subsection with the aid of the system response in terms of $\Delta\omega$, $\Delta\delta$, and V_t of the generator.

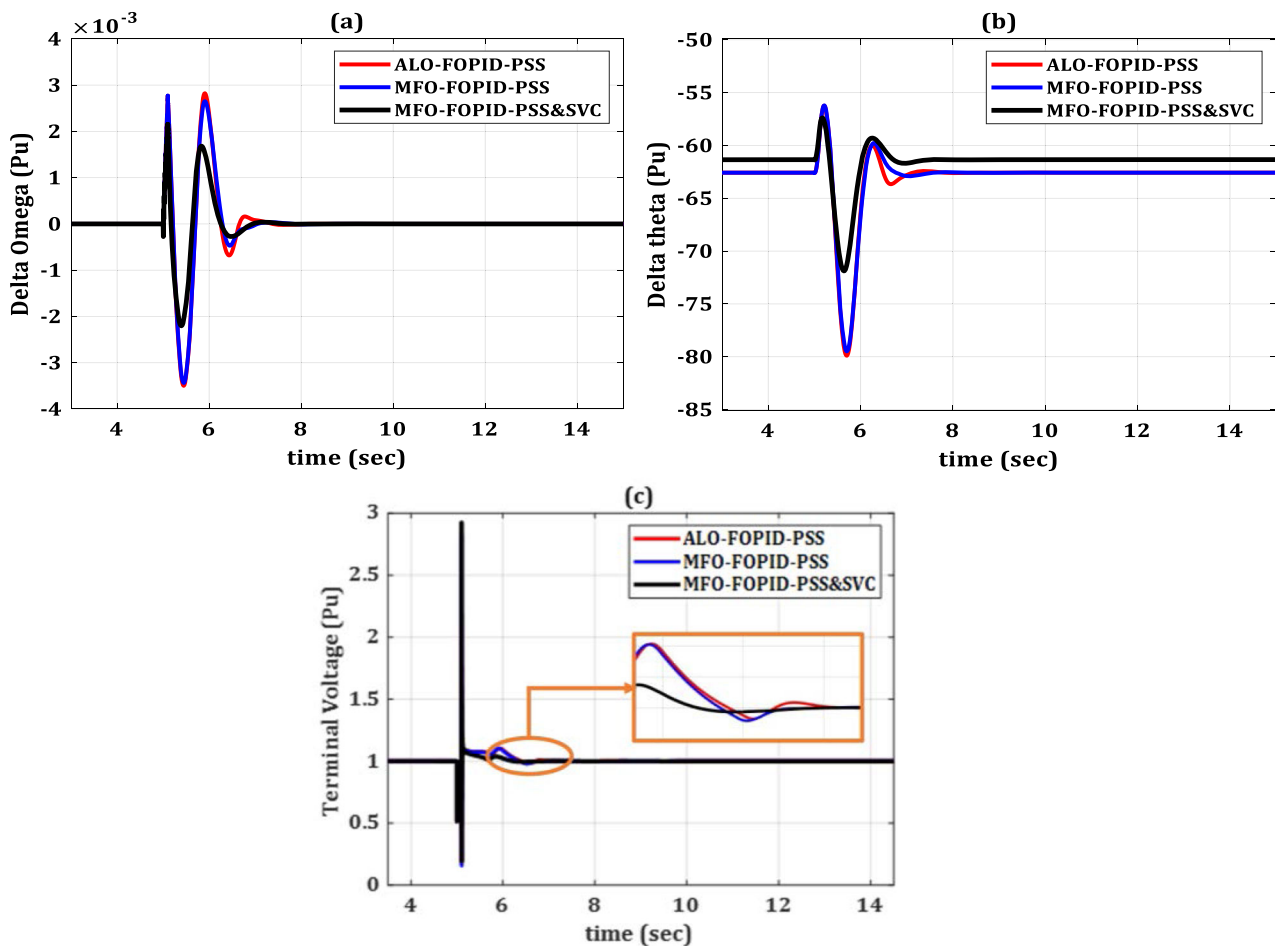


Fig. 15 Response of $\Delta\omega$, $\Delta\delta$, and $V_t(p.u.)$ to test scenario No. 6

5.2.1 Case study no. 1–test scenario no. 4.

The most severe case, symmetrical fault, has been covered in case study No. 1. Figure 14 shows the corresponding signals ($\Delta\omega$, $\Delta\delta$, and V_t) of the simulated case. The depicted signals represent the behavior of each controller in response to the LLL-G fault. As can be seen, the proposed coordinated controller MFO-FOPID-PSS&SVC dramatically improves the power system dynamic stability and has a higher capacity for damping power system oscillations than other controllers. Figure 14a reports that the settling times of these oscillations are about 7.1 s for a coordinated controller, 7.3 s for MFO-FOPID-PSS, and 7.9 s for ALO-FOPID-PSS, which emphasizes that the well-adjusted proposed coordinated controller can provide sufficient damping to the system oscillatory modes.

5.2.2 Case study no. 2–test scenario no. 6.

In case No. 2, an L-G fault has been applied at the generation terminals. Figure 15 shows the system response

to a minor disturbance. The figure shows that the system response with the proposed coordinated controller MFO-FOPID-PSS&SVC has good damping characteristics to low-frequency oscillations than MFO-FOPID-PSS and ALO-FOPID-PSS stabilizers. Moreover, shown in Fig. 15-a, the developed method has lower overshoots than other methods. The overshoots are 0.2155, 0.2772, and 0.2823 p.u for the coordinated controller MFO-FOPID-PSS&SVC, MFO-FOPID-PSS, and ALO-FOPID-PSS, respectively. Hence, the simulation results emphasized the superiority of a coordinated controller MFO-FOPID-PSS&SVC.

5.2.3 Case study no. 3–test scenario no. 11.

A double-line-to-ground fault at the generation terminals has been covered in this case. Figure 16 illustrates the system's speed deviation and rotor angle deviation signals under study. The responses illustrated in Fig. 16 represent the responses of all adopted controllers in this study for the LL-G fault. It can be noticed that the proposed coordinated controller MFO-FOPID-PSS&SVC achieves a better dynamic

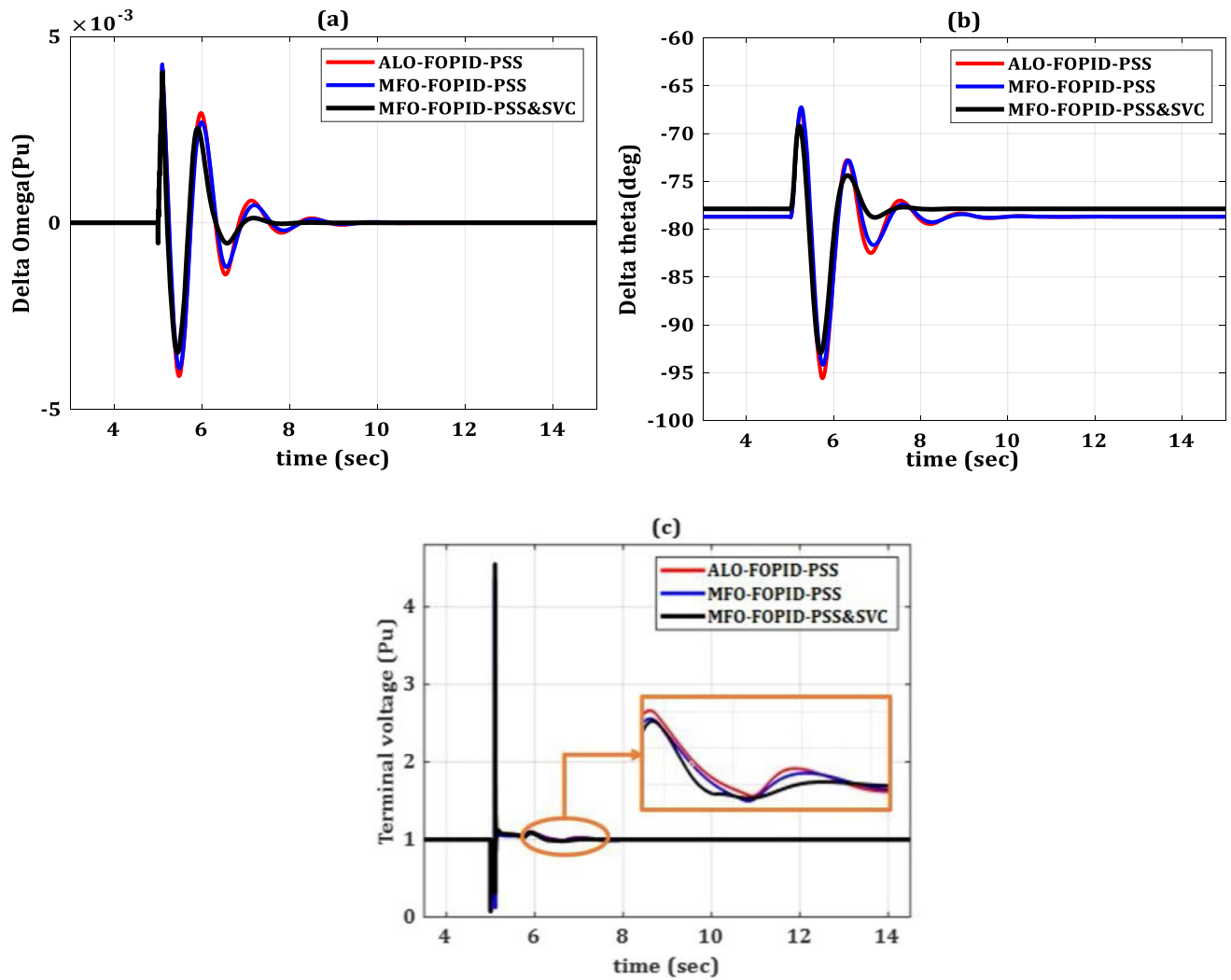


Fig. 16 Response of $\Delta\omega$, $\Delta\delta$, and $V_t(p.u.)$ to test scenario No. 11

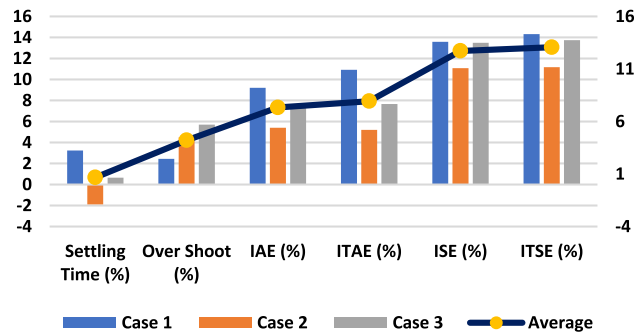


Fig. 17 MFO performance outperformed ALO algorithm for FOPID controller in percentage

response. From Fig. 16a, the settling time and overshoot are **8.678 s** and **0.4249 p.u** for ALO-FOPID-PSS, **8.6216 s** and **0.4247 p.u** for MFO-FOPID-PSS, and **7.3711 s** and **0.4026 p.u** for coordinated design MFO-FOPID-PSS&SVC. Thus, the robustness and effectiveness of the proposed controller

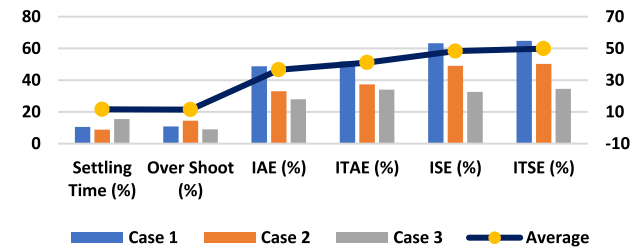


Fig. 18 MFO-FOPID-PSS&SVC performance outperformed MFO-FOPID-PSS in percentage

are proved, considering that obtained settling time and overshoot of the proposed method are less than other controllers.

5.3 Analysis of the results.

Figures 17 and 18 summarize the performance comparison of all adopted controllers in this study. The arithmetic

means was adopted and calculated for all cases to summarize the performance of each controller. Figure 17 shows the performance of the MFO algorithm compared with the ALO algorithm, and Fig. 18 shows the coordinated FOPID-PSS&SVC compared with the FOPID-PSS controller.

The results show that considering all study cases, the FOPID-PSS-based methodology design significantly performs better than LL-PSS and PID-PSS. Furthermore, the performance indices for FOPID-PSS are the most minor compared with other controllers. These significant reductions in performance indices values ensure the robustness and effectiveness of the developed method. Consequently, the proposed controller offers the system excellent performance in maintaining the system stability and damping the oscillations than other controllers.

6 Conclusion

The purpose of this research was to determine the best settings for a power system stabilizer (PSS) based on a coordinated fractional-order proportional-integral-derivative (FOPID) and a static variable-reluctance (var) compensator (SVC). The moth flame optimization technique was adopted to optimize the parameters of both controllers and achieve a coordinated operation between devices. The objective function is formulated in this study based on the integral time absolute of the error (ITAE), and various performance indices were applied to analyze the performance of the proposed controller. The proposed moth flame-based coordinated FOPID and SVC combination has been compared with lead-lag, proportional-integral-derivative (PID), and antlion-based coordinated FOPID with SVC controllers. The comparison and various simulation scenarios were performed, and results were analyzed and reported. The results analysis has revealed that the proposed coordinated controller PSS&SVC-FOPID-POD improved the power system stability higher than the other controllers. The performance indices, settling time, overshoot, IAE, ITAE, ISE, and ITSE, have improved by **11.61%**, **11.45%**, **36.58%**, **41.07%**, **48.32%**, and **49.86%**, respectively, compared with MFO-FOPID-PSS without SVC.

In a few words, the study shows that using the MFO-based FOPID control scheme for both PSS and SVC guarantees much excellent stability of the system and oscillation damping capability.

Authors' contributions HEMA and NMAI prepared the main idea and the methodology. BAH and EAE-s presented the proposed AI algorithm and applied the optimization process. NMAI and EAE-s apply the testing methods and the result analysis. HEMA and BAH check the results and apply numerical investigation to the analysis. NMAI and EAE-s wrote the draft manuscript. HEMA, NMAI, and BAH reviewed the manuscript. All authors read and approved the final manuscript.

Funding Open access funding provided by The Science, Technology & Innovation Funding Authority (STDF) in cooperation with The Egyptian Knowledge Bank (EKB).

Data availability The data that support the findings of this study are available from the first author, upon reasonable request.

Declarations

Conflict of interest The authors declare that they have no competing interests.

Open Access This article is licensed under a Creative Commons Attribution 4.0 International License, which permits use, sharing, adaptation, distribution and reproduction in any medium or format, as long as you give appropriate credit to the original author(s) and the source, provide a link to the Creative Commons licence, and indicate if changes were made. The images or other third party material in this article are included in the article's Creative Commons licence, unless indicated otherwise in a credit line to the material. If material is not included in the article's Creative Commons licence and your intended use is not permitted by statutory regulation or exceeds the permitted use, you will need to obtain permission directly from the copyright holder. To view a copy of this licence, visit <http://creativecommons.org/licenses/by/4.0/>.

Appendix 1

Parameter	Value
Machine damping coefficient, D	0
Inertia constant, M	7.4
Open-circuit field time constant, T'_{do}	4.4529 s
Transient reactance d -axis, X'_d	0.296 p.u
Synchronous reactance d -axis, X_d	1.305 p.u
Synchronous reactance q -axis, X_q	0.474 p.u
Synchronous speed, ω_b (rad/s)	377 rad/s
Gain of SVC, K_{svc}	12
SVC inductive reactance, XL	0.4925 p.u
Initial firing angle α	150°
Gain of excitation system, KA	200
Time constant of excitation system, TA	0.001 s
reactance of transmission line, $X_{l1} = X_{l2}$	0.3 p.u
Transformer reactance X_{tr}	0.1 p.u
Terminal voltage, V_t	1 p.u
Infinite bus voltage, V_b	1 p.u
Resistance of transmission line, Re	0.07

Parameter	Value
Time constant of SVC, T_{svc}	0.025 s
SVC capacitive reactance, XC	1.17 p.u
Washout time constant, T_w	20 s

References

- Chaib L, Choucha A, Arif S (2017) Optimal design and tuning of novel fractional order PID power system stabilizer using a new metaheuristic Bat algorithm. *Ain Shams Eng J*. <https://doi.org/10.1016/j.asej.2015.08.003>
- Arya Y et al (2021) Cascade- $I^\lambda D^\mu N$ controller design for AGC of thermal and hydro-thermal power systems integrated with renewable energy sources. *IET Renew Power Gener* 15(3):504–520. <https://doi.org/10.1049/rpg2.12061>
- P. Kundur, *Power system stability and control by Prabha Kundur.pdf*. 1994.
- Bayu ES, Khan B, Ali ZM, Alaas ZM, Mahela OP (2022) Mitigation of low-frequency oscillation in power systems through optimal design of power system stabilizer employing ALO. *Energies (Basel)* 15(10):3809. <https://doi.org/10.3390/en15103809>
- S. M. H. Hosseini, J. Olamaee, and H. Samadzadeh, "Power oscillations damping by static var compensator using an adaptive neuro-fuzzy controller," in *ELECO 2011–7th International Conference on Electrical and Electronics Engineering*, 2011.
- Mondal D, Chakrabarti A, Sengupta A (2020) Coordinated frequency control strategy for VSC-HVDC-connected wind farm and battery energy Storage system. *Power Syst Small Signal Stability Anal Contr*. <https://doi.org/10.1016/C2018-0-02439-1>
- Kundur P, Klein M, Rogers GJ, Zywno MS (1989) Application of power system stabilizers for enhancement of overall system stability. *IEEE Trans Power Syst* 4:2. <https://doi.org/10.1109/59.193836>
- Lei X, Lerch EN, Povh D (2001) Optimization and coordination of damping controls for improving system dynamic performance. *IEEE Trans Power Syst* 16(3):284. <https://doi.org/10.1109/59.932284>
- Padiyar KR, Kulkarni AM (1997) Flexible AC transmission systems: a status review. *Sadhana* 22(6):845. <https://doi.org/10.1007/BF02745845>
- Dey P, Mitra S, Bhattacharya A, Das P (2019) Comparative study of the effects of SVC and TCSC on the small signal stability of a power system with renewables. *J Renew Sustain Energy* 11:3. <https://doi.org/10.1063/1.5085066>
- Chen JH, Lee WJ, Chen MS (1999) Using a static var compensator to balance a distribution system. *IEEE Trans Ind Appl* 35:2. <https://doi.org/10.1109/28.753620>
- Moghadam AT, Aghahadi M, Eslami M, Rashidi S, Arandian B, Nikolovski S (2022) Adaptive rat swarm optimization for optimum tuning of SVC and PSS in a power system. *Int Trans Electr Energy Syst*. <https://doi.org/10.1155/2022/4798029>
- Welhazi Y et al (2022) A novel hybrid chaotic Jaya and sequential quadratic programming method for robust design of power system stabilizers and static VAR compensator. *Energies (Basel)* 15(3):150. <https://doi.org/10.3390/en15030860>
- H. R. Heydari, H. S. Ali, B. Mahani, and R. Dahim, "Coordinated Designing Between Pss and Svc Pod Controller Using De Algorithm," *International Journal on Technical and Physical Problems of Engineering*, no. September, 2014.
- Kamari NAM, Musirin I, Ibrahim AA (2020) "Swarm intelligence approach for angle stability improvement of PSS and SVC-based SMIB. *J Electr Eng Technol* 15(3):386. <https://doi.org/10.1007/s42835-020-00386-w>
- Abido MA, Abdel-Magid YL (2003) Coordinated design of a PSS and an SVC-based controller to enhance power system stability. *Int J Electr Power Energy Syst* 25(9):124. [https://doi.org/10.1016/S0142-0615\(02\)00124-2](https://doi.org/10.1016/S0142-0615(02)00124-2)
- Keskes S, Sallem S, Kammoun MBA (2021) Nonlinear coordinated control design of generator excitation and static Var compensator for power system via input-output linearization. *Trans Inst Meas Contr* 43:1. <https://doi.org/10.1177/0142331220964361>
- Bian XY, Tse CT, Zhang JF, Wang KW (2011) Coordinated design of probabilistic PSS and SVC damping controllers. *Int J Electr Power Energy Syst* 33:3. <https://doi.org/10.1016/j.ijepes.2010.10.006>
- Peres W (2019) Multi-band power oscillation damping controller for power system supported by static VAR compensator. *Electr Eng*. 101:3. <https://doi.org/10.1007/s00202-019-00830-9>
- Abdulrahman I, Radman G (2019) Simulink-based programs for power system dynamic analysis. *Electr Eng* 10:2. <https://doi.org/10.1007/s00202-019-00781-1>
- Falehi AD, Rostami M, Doroudi A, Ashrafiyan A (2012) Optimization and coordination of SVC-based supplementary controllers and PSSs to improve power system stability using a genetic algorithm. *Turkish J Electr Eng Comput Sci* 20(5):838. <https://doi.org/10.3906/elk-1010-838>
- Saadatmand M, Gharehpetian GB, Kamwa I, Siano P, Guerrero JM, Alhelou HH (2021) A survey on fopid controllers for lfo damping in power systems using synchronous generators, facts devices and inverter-based power plants. *Energies* 14(18):983. <https://doi.org/10.3390/en14185983>
- Nidhi S, Mahesh S, Shimp R (2020) Performance analysis of hybrid controller in SMIB system using metaheuristic optimization techniques under different design criteria. *Manag J Future Eng Technol* 16(1):11. <https://doi.org/10.26634/jfet.16.1.17384>
- El-Dabah MA, Kamel S, Abido MAY, Khan B (2022) Optimal tuning of fractional-order proportional, integral, derivative and tilt-integral-derivative based power system stabilizers using Runge Kutta optimizer. *Eng Rep* 4(6):1024. <https://doi.org/10.1002/eng2.12492>
- E. S. Ali and S. M. Abd-Elazim, (2014) Power system stability enhancement via new coordinated design of PSSs and SVC. *WSEAS Transactions on Power Systems* 9
- .Kumar, A. Kumar, and G. Shankar, "Crow search algorithm based optimal dynamic performance control of SVC assisted SMIB system," in *2018 20th National Power Systems Conference, NPSC 2018*, 2018. doi: <https://doi.org/10.1109/NPSC.2018.8771814>.
- Filho RND, Paucar VL (2018) Robust and coordinated tuning of PSS and FACTS-PODs of interconnected systems considering signal transmission delay using ant lion optimizer. *J Contr Auto Electr Syst*. <https://doi.org/10.1007/s40313-018-0408-5>
- P. Dey, A. Bhattacharya, and P. Das, Tuning of power system stabilizers in multi-machine power systems using moth flame optimization. In: *IEEECON 2018–6th international electrical engineering congress*, 2018. doi: <https://doi.org/10.1109/IEEECON.2018.8712306>.
- Shin Mei RN, Sulaiman MH, Daniyal H, Mustaffa Z (2018) Application of moth-flame optimizer and ant lion optimizer to solve optimal reactive power dispatch problems. *J Telecommun Electr Comput Eng* 10:1–2
- Nandi M, Shiva CK, Mukherjee V (2020) Moth-flame algorithm for TCSC- and SMES-based controller design in automatic generation control of a two-area multi-unit hydro-power system. *Iranian J Sci Technol Trans Electr Eng*. <https://doi.org/10.1007/s40998-019-00297-1>

31. Yadykin IB, Tomin NV, Iskakov AB, Galyaev IA (2022) Optimal adaptive control of electromechanical oscillations modes in power systems. IFAC-PapersOnLine. <https://doi.org/10.1016/j.ifacol.2022.07.024>
32. Çelik E (2021) Design of new fractional order PI–fractional order PD cascade controller through dragonfly search algorithm for advanced load frequency control of power systems. *Soft comput* 25(2):1193–1217. <https://doi.org/10.1007/s00500-020-05215-w>
33. Arya Y, Dahiya P, Çelik E, Sharma G, Gözde H, Nasiruddin I (2021) AGC performance amelioration in multi-area interconnected thermal and thermal-hydro-gas power systems using a novel controller. *Eng Sci Technol Int J* 24(2):384–396. <https://doi.org/10.1016/j.jestch.2020.08.015>
34. Çelik E, Öztürk N (2022) Novel fuzzy 1PD-TI controller for AGC of interconnected electric power systems with renewable power generation and energy storage devices. *Eng Sci Technol Int J* 35:101166. <https://doi.org/10.1016/j.jestch.2022.101166>
35. P. C. Sahu, R. C. Prusty, and S. Panda, ALO optimized NCTF controller in multi area AGC system integrated with WECS based DFIG system. In: *proceedings of IEEE international conference on circuit, power and computing technologies, ICCPCT 2017*, 2017. doi: <https://doi.org/10.1109/ICCPCT.2017.8074377>.
36. P. C. Sahu, R. C. Prusty, and S. Panda, “MFO algorithm based fuzzy-PID controller in automatic generation control of multi-area system. In: *proceedings of IEEE international conference on circuit, power and computing technologies, ICCPCT 2017*, 2017. doi: <https://doi.org/10.1109/ICCPCT.2017.8074316>
37. Sahu PC, Prusty RC, Panda S (2019) A gray wolf optimized FPD plus (1+PI) multistage controller for AGC of multisource nonlinear power system. *World J Eng.* <https://doi.org/10.1108/WJE-05-2018-0154>
38. P. C. Sahu, B. Begum, R. C. Prusty, B. K. Sahu, and M. K. Devnath, “A grasshopper optimized FO- multistage controller for frequency control of an AC microgrid. In *Ist odisha international conference on electrical power engineering, communication and computing technology, ODICON 2021*, 2021. doi: <https://doi.org/10.1109/ODICON50556.2021.9428981>.
39. M. Hassan, M. A. Abido, and A. Aliyu, “Design of power system stabilizer using phase based objective function and heuristic algorithm. *Sin 2019 8th international conference on modeling simulation and applied optimization, ICMSAO 2019*, 2019. doi: <https://doi.org/10.1109/ICMSAO.2019.8880343>.
40. Ibrahim NMA, Attia HEM, Talaat HEA, Alaboudy AHK (2015) Modified particle swarm optimization based proportional-derivative power system stabilizer. *Int J Intell Syst Appl* 7(3):62–76. <https://doi.org/10.5815/ijisa.2015.03.08>
41. Tiako R, Folly KA (2009) Investigation of power system stabiliser parameters optimisation using multi-power flow conditions. *Aust J Electr Electron Eng.* <https://doi.org/10.1080/1448837x.2008.11464216>
42. Ibrahim NMA, Elnaghi BE, Ibrahim HA, Talaat HEA (2019) Modified particle swarm optimization based on lead-lag power system stabilizer for improve stability in multi-machine power system. *Int J Electr Eng Inform.* <https://doi.org/10.15676/ijeeci.2019.11.1.10>
43. Ibrahim NMA, Elnaghi BE, Ibrahim HA, Talaat HEA (2018) Modified particle swarm optimization based on lead-lag power system stabilizer for improve stability in multi-machine power system. *Int J Electr Eng Inform* 11(1):161–182. <https://doi.org/10.15676/ijeeci.2019.11.1.10>
44. Behzadpoor S, Davoudkhani IF, Abdelaziz AY, Geem ZW, Hong J (2022) Power system stability enhancement using robust FACTS-based stabilizer designed by a hybrid optimization algorithm. *Energies (Basel).* <https://doi.org/10.3390/en15228754>
45. Kalegowda K, Srinivasan ADI, Chinnamadha N (2022) Particle swarm optimization and Taguchi algorithm-based power system stabilizer-effect of light loading condition. *Int J Electr Comput Eng.* <https://doi.org/10.11591/ijece.v12i5.pp4672-4679>
46. Dasu B, Sivakumar M, Srinivasarao R (2019) Interconnected multi-machine power system stabilizer design using whale optimization algorithm. *Protect Contr Modern Power Syst.* <https://doi.org/10.1186/s41601-019-0116-6>
47. F. G. Martins, “Tuning PID controllers using the ITAE criterion,” *International Journal of Engineering Education*, vol. 21, no. 5 PART I AND II, 2005.
48. Kalyan CNS, Suresh CV, Ramaniah U (2022) Multi-objective weighted-sum optimization for stability of dual-area power system using water cycle algorithm. *Lecture Notes Electr Eng.* https://doi.org/10.1007/978-981-16-6970-5_2
49. Barakat M (2022) Optimal design of fuzzy-PID controller for automatic generation control of multi-source interconnected power system. *Neural Comput Appl.* <https://doi.org/10.1007/s00521-022-07470-4>
50. Jovcic D, Pillai GN (2005) Analytical modeling of TCSC dynamics. *IEEE Trans Power Delivery.* <https://doi.org/10.1109/TPWRD.2004.833904>
51. A. K. Patra, S. K. Mohapatra, and S. K. Barik, “Coordinated Design of SVC based Power System Stabilizer using Pattern Search Algorithm,” in *Proceedings of the 2020 International Conference on Renewable Energy Integration into Smart Grids: A Multidisciplinary Approach to Technology Modelling and Simulation, ICREISG 2020*, 2020. doi: <https://doi.org/10.1109/ICREISG49226.2020.9174556>.
52. H. F. Wang, “A unified model for the analysis of FACTS devices in damping power system oscillations-Part III: Unified power flow controller,” *IEEE Transactions on Power Delivery*, vol. 15, no. 3, 2000, doi: <https://doi.org/10.1109/61.871362>.
53. H. Wang and W. Du, *Analysis and Damping Control of Power System Low-frequency Oscillations*. 2016.
54. Farah A et al (2021) A new design method for optimal parameters setting of pss and svc damping controllers to alleviate power system stability problem. *Energies (Basel)* 14(21):12. <https://doi.org/10.3390/en14217312>
55. H. Shayeghi, H. A. Shayanfar, S. Asefi, and A. Younesi, Optimal tuning and comparison of different power system stabilizers using different performance indices Via Jaya Algorithm. In: *Int’l conf. scientific computing (CSC’16)*, Computer engineering and applied computing (WorldComp), 2016, p. 34.
56. Mijbas AF, Hasan BAA, Salah HA (2020) Optimal stabilizer PID parameters tuned by chaotic particle swarm optimization for damping low frequency oscillations (LFO) for single machine infinite bus system (SMIB). *J Electr Eng Technol* 15(4):442. <https://doi.org/10.1007/s42835-020-00442-5>
57. Sayed Y, Ahmed A-H, Elghaffar AA, Eltamaly A (2019) Multi-shunt VAR compensation SVC and STATCOM for enhance the power system quality. *J Electr Eng* 19:12
58. Biswas MM, Das KK (2011) Voltage level improving by using static VAR compensator (SVC). *Global J Res Eng* 11(5):13–18
59. Kazemi A, Badrzadeh B (2004) Modeling and simulation of SVC and TCSC to study their limits on maximum loadability point. *Int J Electr Power Energy Syst.* 26(8):8. <https://doi.org/10.1016/j.ijepes.2004.04.008>
60. Taha IBM “Best locations of shunt SVCs for steady state voltage stability enhancement. In *2015 IEEE conference on energy conversion, CENCON 2015*, 2015. doi: <https://doi.org/10.1109/CENCON.2015.7409583>.
61. Suresh V, Sreejith S (2017) Power flow analysis incorporating renewable energy sources and FACTS devices. *Int J Renew Energy Re* 7(1):7019. <https://doi.org/10.20508/ijrer.v7i1.5074.g7019>

62. Benayad K, Zabaoui T, and Bouafassa A, Wide-area based SVC-Fractional order PID controller for damping inter-area oscillations. In: 6th IEEE international energy conference, ENERGY-Con 2020, 2020. doi: <https://doi.org/10.1109/ENERGYCon48941.2020.9236492>.
63. Hasanvand H, Bakhshideh Zad B, Mozafari B, Feizifar B (2013) Damping of low-frequency oscillations using an SVC-based supplementary controller. *IEEJ Trans Electr Electron Eng* 8(6):895. <https://doi.org/10.1002/tee.21895>
64. Mirjalili S (2015) The ant lion optimizer. *Adv Eng Softw* 83:10. <https://doi.org/10.1016/j.advengsoft.2015.01.010>
65. Ibrahim NMA, Talaat HEA, Shaheen AM, Hemade BA (2023) Optimization of power system stabilizers using proportional-integral-derivative controller-based antlion algorithm: experimental validation via electronics environment. *Sustainability* 15(11):8966. <https://doi.org/10.3390/su15118966>
66. Devarapalli R, Bhattacharyya B, Saw JK (2020) Controller parameter tuning of a single machine infinite bus system with static synchronous compensator using antlion optimization algorithm for the power system stability improvement. *Adv Contr Appl Eng Industr Syst* 2(3):45. <https://doi.org/10.1002/adc2.45>
67. Mirjalili S (2015) Moth-flame optimization algorithm: a novel nature-inspired heuristic paradigm. *Knowl Based Syst* 89:228–249. <https://doi.org/10.1016/j.knosys.2015.07.006>
68. Bibhuti BP and Bidyadhar R, MFO Ptimized fractional order based controller on power system stability. In: proceedings of engineering and technology innovation, Taiwan: Association of Engineering and Technology Innovation, Apr. 2018, pp. 46–59.
69. Alzaqebah M, Alrefai N, Ahmed EAE, Jawarneh S, Alsmadi MK (2020) Neighborhood search methods with moth optimization algorithm as a wrapper method for feature selection problems. *Int J Electr Comput Eng* 10(4):3684. <https://doi.org/10.11591/ijece.v10i4.pp3672-3684>

Publisher's Note Springer Nature remains neutral with regard to jurisdictional claims in published maps and institutional affiliations.